4D full-field measurements over the entire loading history: Evaluation of different temporal interpolations

Ana Vrgoč[1,2], Viktor Kosin[2,3], Clément Jailin[4], Benjamin Smaniotto[2],
Zvonimir Tomičević[*1] and François Hild[2]

[1]*Laboratory of Experimental Mechanics, Faculty of Mechanical Engineering and Naval Architecture,
University of Zagreb, Ivana Lučića 5, 10002, Zagreb, Croatia*
[2]*Université Paris-Saclay, CentraleSupélec, ENS Paris-Saclay, CNRS
LMPS−Laboratorie de Mécanique Paris-Saclay, Gif-sur-Yvette, France*
[3]*Leibniz Universität Hannover, Institut für Angewandte Mathematik (IFAM), Hannover, Germany*
[4]*GE HealthCare, Buc, France*

Abstract. Standard Digital Volume Correlation (DVC) approaches are based on pattern matching between two reconstructed volumes acquired at different stages. Such frameworks are limited by the number of scans (due to acquisition duration), and time-dependent phenomena can generally not be captured. Projection-based Digital Volume Correlation (P-DVC) measures displacement fields from series of 2D radiographs acquired at different angles and loadings, thus resulting in richer temporal sampling (compared to standard DVC). The sought displacement field is decomposed over a basis of separated variables, namely, temporal and spatial modes. This study utilizes an alternative route in which spatial modes are con-structed via scan-wise DVC, and thus only the temporal amplitudes are sought via P-DVC. This meth-od is applied to a glass fiber mat reinforced polymer specimen containing a machined notch, subjected to in-situ cyclic tension, and imaged via X-Ray Computed Tomography. Different temporal interpolations are exploited. It is shown that utilizing only one DVC displacement field (as spatial mode) was sufficient to properly capture the complex kinematics up to specimen failure.

1. Introduction

Due to their advantageous material properties and unique ability to tailor them to meet specific design requirements, fiber reinforced polymers (FRPs) are increasingly being regarded as efficient substitutes for conventional engineering materials in critical-safety and lightweight structural applications (Prashanth *et al.* 2017). The failure of such materials is induced by various damage mechanisms, which initiate at different length scales and often interact (Brunner 2018, Vrgoč *et al.* 2021). These phenomena call for advanced techniques for damage detection and quantification. X-Ray Computed Tomography (XCT) has proven to be a powerful tool in experimental solid

---

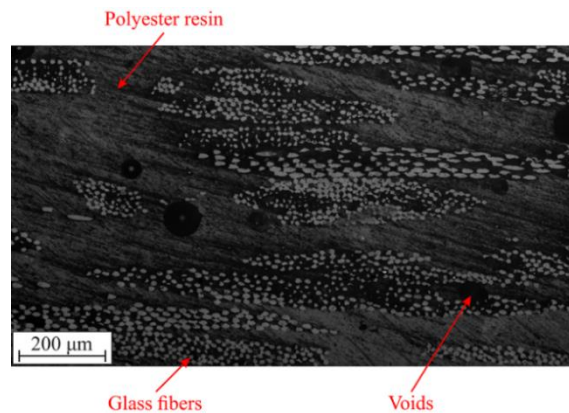∗Corresponding author, Professor, E-mail: zvonimir.tomicevic@fsb.hr

Fig. 1 Optical micrograph of the glass fiber mat reinforced polyester resin composite studied herein

mechanics to assess bulk kinematics and microstructural changes (Buljac *et al.* 2018a, Buljac *et al.* 2018b, Tomičević *et al.* 2019). When coupled with Digital Volume Correlation (DVC), quantitative analyses of specimen deformation can be performed *in-situ* between two discrete states. However, the material behavior between two consecutive scans is not accessible (as acquisitions may last for few minutes up to few hours). Thus, time-dependent phenomena (such as creep or relaxation) cannot be captured. As FRPs are likely to undergo stress relaxation during experiments (Maurer *et al.* 2022, Vrgoč *et al.* 2023), the reconstructed volumes may be impacted by motion artifacts. These restrictions can be circumvented by performing 4D (i.e., space and time) measurements employing the recently developed Projection-based Digital Volume Correlation (P-DVC). Instead of working with fully reconstructed volumes, P-DVC measures displacement fields from series of 2D radiographs acquired at different angles and loadings, thereby resulting in richer temporal resolutions without degrading too much the spatial resolution (Buljac *et al.* 2018, Jailin *et al.* 2018a). In general, P-DVC relies on space-time discretizations of displacement fields (Jailin *et al.* 2018a). The following study utilizes an alternative route in which spatial modes are constructed via scan-wise DVC, and thus only the corresponding temporal modes are sought via P-DVC.

The present work aims for 4D (i.e., space and time) characterizations of a glass fiber mat reinforced polyester resin subjected to *in-situ* cyclic tension. The dogbone specimen (containing a machined rectangular notch to induce high strain gradients) was subjected to cyclic tensile loading and simultaneously imaged in an XCT scanner. First, the properties and fabrication procedure of the investigated composite are presented, followed by a brief description of P-DVC in which the spatial modes are described by DVC fields. The investigated specimen geometry is presented together with the employed mechanical and imaging setup. Finally, the results of 4D measurements are discussed.

2. Material and experimental setup

The investigated material is a polyester resin reinforced with a continuous glass fiber mat. It was produced by manual lay-up followed by compression molding. The laminate consisted of 12 plies of R-glass fiber mat. The composition (in volume fraction) was 40% of fibers, 55% of matrix

Table 1 Scanning parameters

Tomograph	North Star Imaging X50+	
X-ray source	XRayWorX XWT-240-CT	
Target / Anode	W (reflection mode)	
Filter	None	
Voltage	145 kV	
Current	78 μA	
Focal spot size	5 μm	
Tube to detector	910 mm	
Detector	Dexela 2922	
Definition	1507×1849 px (2×2 binning)	
Scanning parameters	High quality (HQ)	Low quality (LQ)
Number of projections	800	768
Angular amplitude	360°	360°
Frame average	20 per projection	Continuous (1 per projection)
Frame rate	3 fps	3 fps
Acquisition duration	1 h 46 min 26 s	4 min 26 s
Reconstruction algorithm	Filtered back-projection	Filtered back-projection
Gray levels amplitude	8 bits	8 bits
Field of view	7.3×10×20.5 mm³	7.3×10×20.5 mm³
Pattern	Natural (Fig. 2(b))	Natural (Fig. 2(b))

and, as vacuum was not applied during molding, the volume fraction of air voids was equal to 5%. The enhanced contrast between the constituents (in this specific case, between matrix, fibers and air voids, as shown in Fig. 1) makes the investigated material suitable for DVC analyses as it relies on natural patterns (Buljac *et al.* 2018, Bartulović *et al.* 2022).

The 5.2 mm thick dogbone specimen contained a machined rectangular notch to induce high strain gradients (Fig. 2(a)). The notch depth was 1.6 mm and its width was equal to 0.6 mm. The radiographs were acquired continuously over the entire loading history in the X50+ scanner (North Star Imaging) of LMPS. First, the reference volume was acquired in the unloaded state (marked with black dots in Fig. 3). This scan consisted of 800 radiographs captured at equally spaced angles ranging over a full 360° revolution, and was acquired with so-called high quality (HQ) scanning parameters (Table 1). This acquisition took approximately 2 h to be completed. To conduct the experiment in a reasonable time and to mitigate e.g., stress-relaxation, the number of averaging frames for all subsequent acquisitions was lowered to 1 (i.e., continuous scanning parameters). The latter settings led to 4 min acquisitions per revolution. After acquiring the reference scan, the specimen was subjected to cyclic tension at a constant stroke velocity of 4μm/s, and a continuous rotation of the specimen was set with 768 acquisitions per turn (see the so-called low quality (LQ) parameters in Table 1). The radiographs were continuously acquired during the prescribed loading history with angular increments of 0.46°.

The deformed scans were reconstructed from the stages where a constant stroke was applied (marked with red dots in Fig. 3). These scans were used to calculate displacement fields via finite
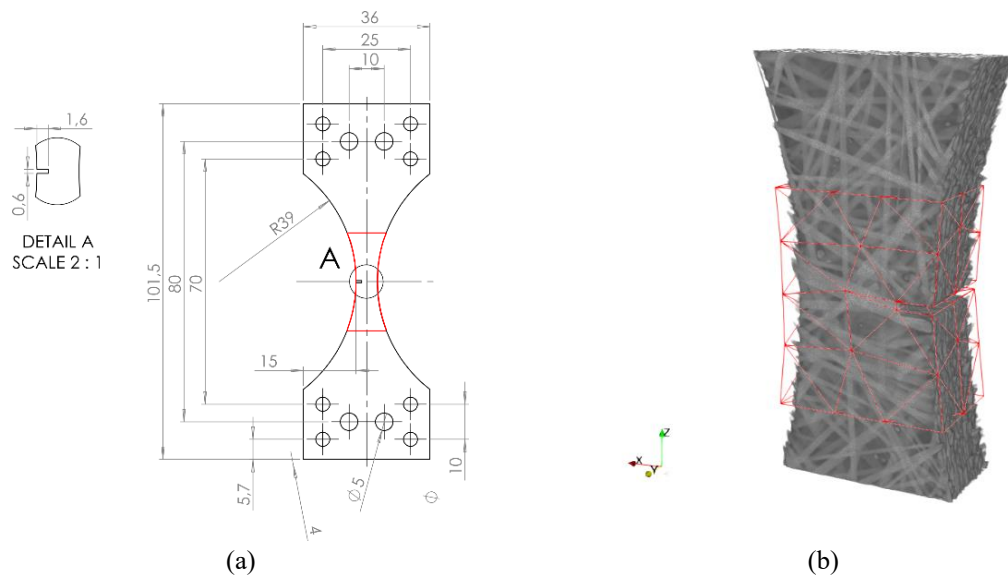
Fig. 2 (a) Geometry of the investigated single notched dogbone specimen together with the Region of Interest (depicted with red contour), the size of which is 384×384×486 vx. The dimensions are expressed in mm. (b) Reconstructed reference volume together with first-order tetrahedral mesh employed herein
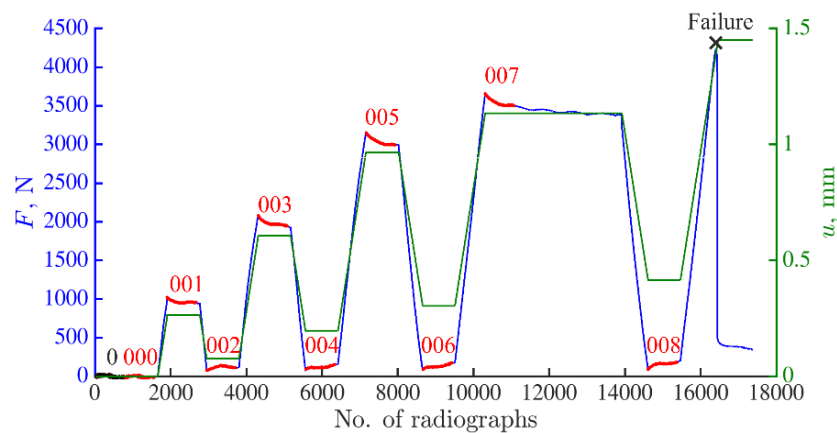

Fig. 3 Measured uniaxial force (blue) and stroke history (green) of the studied *in-situ* tensile test. The black dots mark the acquisition of the high-quality reference scan (0). The red dots depict the load levels at which full volumes were reconstructed. These volumes were employed in the scan-wise DVC analyses

element (FE) based DVC implemented within the Correli 3.0 framework (Leclerc *et al.* 2015). A total of 17,442 projections was acquired during the prescribed loading history. The radiographs had an initial definition of 1944×1536 px. Coarse graining of 4×4 elementary pixels into one superpixel was performed. This down-sampling led to 486×384 px projections (called images at scale 4), while the physical length of one voxel was equal to 58 μm. The volume reconstruction was performed within the ASTRA toolbox (van Aarle *et al.* 2015) employing the geometrical parameters given by tomograph calibration and a filtered back-projection approach. The inspected

Region of Interest (ROI) was discretized with first-order tetrahedral elements tailored to the actual specimen geometry (Fig. 2(b)). The average element length was 20 vx.

3. Projection-based digital volume correlation

This section outlines the basic principles of DVC and P-DVC. The notations used herein are introduced as well. The projections of the volume $f(\mathbf{x})$ (i.e., the sum of absorption coefficient along each material point $\mathbf{x}$ of the beam ray hitting the detector at position $\mathbf{r}$) are denoted as $p(\mathbf{r}, \theta(t))$, with θ the rotation angles at different time t. This results in a linear relationship between f and p

$$\Pi_{\theta(t)}[f(\mathbf{x})] = p(\mathbf{r}, \theta(t)), \tag{1}$$

with $\Pi_{\theta(t)}$ being the projection operator at angle $\theta(t)$. The inversion of this linear system for a large sequence of angles is called reconstruction. The 3D kinematics of a medium can be followed by reconstructing a series of such tomographic images. The full-field displacement field is estimated via DVC, which relies on the conservation of gray levels

$$f^{T_0}(\hat{\mathbf{x}}) = f^T(\hat{\mathbf{x}} + \hat{\mathbf{u}}(\hat{\mathbf{x}}, T)), \tag{2}$$

where $\hat{\mathbf{x}}$ denotes the position of any material point in the reference configuration, and $\hat{\mathbf{u}}$ is the sought displacement field that describes the change of the reference volume f^{T_0} (usually captured in the undeformed state) to the deformed configuration (here marked as f^T). It is important to note the different time scales, i.e., the 3D images are reconstructed over the duration needed for one turn T. To reconstruct such 3D images, hundreds up to thousands instantaneous radiographs (i.e., projections) captured at $\theta(t)$ are needed over a full revolution (or turn) of the specimen. The turn parameter T marks the different states at which a 3D scan was captured, while T_0 simply denotes the reference scan. The sought displacement field is obtained from the minimization of the quadratic differences

$$\hat{\mathbf{u}}(\hat{\mathbf{x}}, T) = Argmin_{\hat{v}} \sum_{\hat{x}} \left(f^T(\hat{\mathbf{x}} + \hat{\mathbf{v}}(\hat{\mathbf{x}}, T)) - f^{T_0}(\hat{\mathbf{x}}) \right)^2. \tag{3}$$

As a global (i.e., FE-based) approach was employed in the present study, the displacement field is written as follows

$$\hat{\mathbf{v}}(\hat{\mathbf{x}}, T) = \sum_j v_j \hat{\boldsymbol{\psi}}_j(\hat{\mathbf{x}}), \tag{4}$$

where v_j are nodal displacements, and $\hat{\boldsymbol{\psi}}_j$ the corresponding FE shape functions. The present DVC framework is Lagrangian since the sought displacement field is determined with respect to the reference configuration.

Instead of utilizing fully reconstructed volumes, P-DVC aims to measure 4D (i.e., space and time) fields from a series of 2D projections acquired at different angles $\theta(t)$ and loading steps (Jailin *et al.* 2018b). The minimization problem is thus rewritten as follows

$$\mathbf{u}(\mathbf{x}, t) = Argmin_v \sum_{r,t} \left(\Pi_{\theta(t)} [f^{T_0}(\mathbf{x} - \mathbf{v}(\mathbf{x}, t))] - p(\mathbf{r}, \theta(t)) \right)^2. \tag{5}$$

Thus, the problem is no longer stated in the Lagrangian framework, but in the Eulerian system (contrary to Eq. (3)). To complete the notations needed to describe the motion in Lagrangian and Eulerian settings, it is worth noting that the displacement at any spatial location $\mathbf{x}$ reads

$$\mathbf{u}(\mathbf{x}, t) = \mathbf{x} - \hat{\mathbf{x}} = \hat{\mathbf{u}}(\hat{\mathbf{x}}, t). \tag{6}$$

The P-DVC method employed herein requires the acquisition of one reference volume f^{T_0}. As the microstructure of the sample is known from f^{T_0}, the remaining unknowns are the displacements sought in the spatiotemporal framework. In the present work, the spatial component is constructed with scan-wise DVC, while only the temporal modes are sought via P-DVC

$$\mathbf{u}(\mathbf{x}, t) = \sum_\tau \alpha_\tau \hat{\mathbf{U}}^{DVC}(\hat{\mathbf{x}}, T)\sigma_\tau(t), \tag{7}$$

where $\sigma_\tau(t)$ gathers temporal basis function(s), α the temporal amplitude(s), while the DVC field reads

$$\hat{\mathbf{U}}^{DVC}(\hat{\mathbf{x}}, T) = \sum_j v_j(T)\hat{\mathbf{\Psi}}_j(\hat{\mathbf{x}}). \tag{8}$$

The displacement fields are thus sought in a vector space generated by a reduced kinematic basis. The interpolation functions σ naturally introduce temporal regularization (Jailin *et al.* 2018b). In such a way, only one projection per loading level is needed. In the present work, the temporal basis $\sigma(t)$ consisted in the stroke history or the measured uniaxial force, and only *one* DVC field was utilized as spatial mode. Thus, the nodal displacements $v_j(T)$ were measured via FE-DVC, and the temporal amplitude is sought via P-DVC and iteratively updated

$$\alpha^{l+1} = \alpha^l + \delta\alpha^l, \tag{9}$$

where the correction is calculated by performing Gauss-Newton minimizations

$$\delta\alpha^l = \frac{m^l}{M^l}. \tag{10}$$

In Eq. (10), the Hessian M^l is updated for each iteration

$$M^l = \sum_t \left(S^l(\mathbf{r}, t)\sigma(t)\right) \cdot \left(S^l(\mathbf{r}, t)\sigma(t)\right), \tag{11}$$

where S is the projected sensitivity

$$S^l(\mathbf{r}, t) = \Pi_{\theta(t)}\left[\hat{\mathbf{U}}^{DVC}(\hat{\mathbf{x}}, T) \cdot \nabla f^{T_0}\left(\mathbf{x} - \mathbf{u}^l(\mathbf{x}, t)\right)\right]. \tag{12}$$

Furthermore, the second member m^l is based on the projected residual fields

$$m^l = \sum_{r,t} S^l(\mathbf{r}, t)\sigma(t)\varphi_C{}^l(\mathbf{r}, \theta(t)), \tag{13}$$

where the projection residual field per angle at each iteration is expressed as

$$\varphi_C{}^l(\mathbf{r}, \theta(t)) = p(\mathbf{r}, \theta(t)) - \Pi_{\theta(t)}\left[f^{T_0}\left(\mathbf{x} - \mathbf{u}^l(\mathbf{x}, t)\right)\right]. \tag{14}$$

Thus, the reference volume, corrected by the displacement field $\mathbf{u}^l(\mathbf{x}, t)$, and projected for each angle $\theta(t)$ should match the acquired projection $p(\mathbf{r}, \theta(t))$. The projection residual field for all angles is to be minimized during the iterative procedure. As in DVC, these residuals reveal what was not captured by the 4D corrections, herein projected in the 2D detector space. A general overview of 4D analyses in which spatial modes are controlled by DVC fields is shown in Algorithm 1.

Algorithm 1 P-DVC enhanced DVC

Perform DVC analysis$\rightarrow \widehat{\mathbf{U}}^{DVC}(\widehat{\mathbf{x}}, T)$

Choose an initial guess α^0

while $|\delta\alpha^l| > 1 \cdot 10^{-3}$ **do**

   Corrections $f^l(\mathbf{x}, t) \leftarrow f^{T_0}\left(\mathbf{x} - \mathbf{u}^l(\mathbf{x}, t)\right)$

   Update M^l and m^l

   Solve $\delta\alpha^l = \dfrac{m^l}{M^l}$

   Update temporal amplitudes $\alpha^{l+1} = \alpha^l + \delta\alpha^l$,

   Update displacement fields $\mathbf{u}^{l+1}(\mathbf{x}, t) = \alpha^{l+1}\widehat{\mathbf{U}}^{DVC}(\widehat{\mathbf{x}}, T)\sigma(t)$

end while

---

4. Application to *in-situ* test on single-notched specimen

In this section, the kinematics of a single-notched specimen subjected to *in-situ* cyclic tension is analyzed. The P-DVC measurements were performed *up to specimen failure*. Prior to performing 4D measurements, the reconstruction errors were evaluated. Then the results of 4D full-field measurements over the *entire* loading history are presented. They all converged, i.e., the change of displacement correction amplitude $\delta\alpha$ (Eq. (10)) between two iterations became less than 10^{-3}.

4.1 Evaluation of reconstruction error

As shown in Eq. (14), the P-DVC code minimizes the projection residual fields, i.e., differences between the acquired radiograph $p(\mathbf{r}, \theta(t))$ and the reference volume corrected by the sought displacement field, and projected according to the angle $\theta(t)$. It is interesting to extend this procedure to the initial state (corresponding to the reference scan 0), where **u** is equal to **0** by
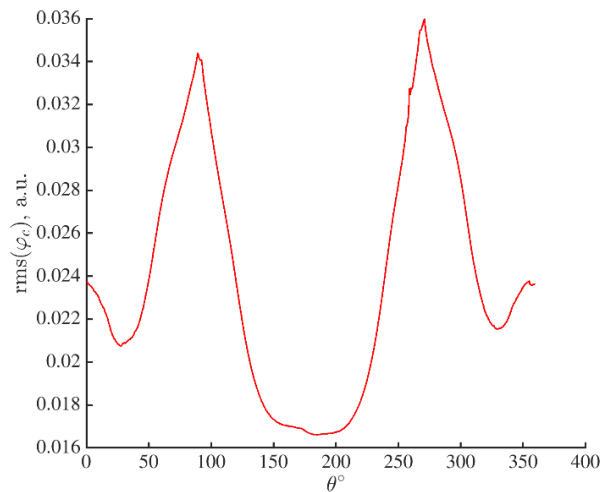

Fig. 4 Root mean square (rms) residuals evaluated for the first 360° revolution (scan 0)
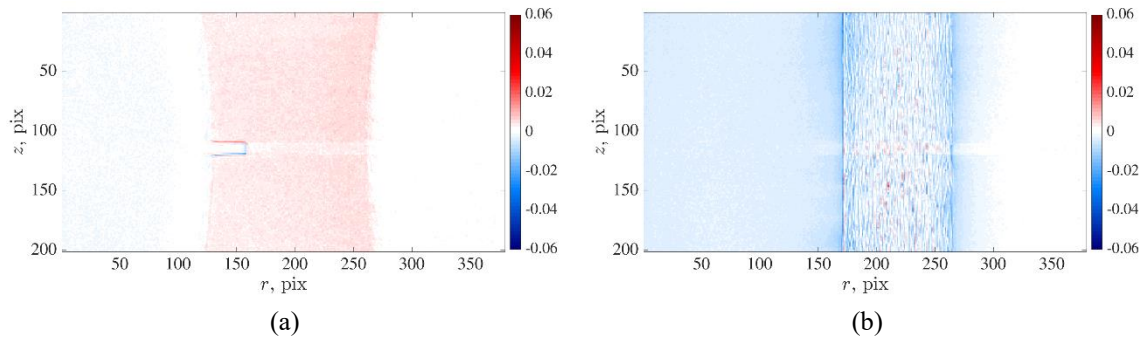
Fig. 5 Initial projection residual fields for (a) $\theta=0°$ and (b) $\theta=90°$

definition. Thus, the reconstruction error was quantified by evaluating the difference between the corresponding projections and re-projections of the reconstructed reference volume 0 (acquired in the unloaded stage, as marked in Fig. 3). Due to acquisition noise, uncertainties in the geometric parameters used for the reconstruction and assumptions in the projection operator (linearity, pixel/voxel integration, …), the initial residual field was not equal to 0. Fig. 4 shows the root mean square (rms) residuals (in arbitrary units) evaluated for the first 360° revolution (scan 0). The residuals were low with respect to the mean dynamic range of the original radiographs (0.7 a.u.).

The highest rms residual levels ($\theta=90°$ and $\theta=270°$) stem from the specimen orientation with respect to the X-ray source (i.e., the thickness of the specimen with respect to the X-ray source was highest at those angles, which influenced X-ray attenuation). The projection residual fields for two different angles are presented in Fig. 5. These initial residual maps are shown with a divergent colormap to highlight positive and negative values. The initial residual field for $\theta=0°$ revealed elevated levels close to the edges of the notch. The residual could be reduced by further adjusting the geometric parameters of the tomography setup. Another source for such error could be small motions during scanning or beam hardening. The latter was not corrected in the present work.

4.2 Full-field measurements over the entire loading history

First, the 4D kinematics was measured using the normalized force signal as temporal basis. As shown in Fig. 3, the measured uniaxial force history highlighted rapid but limited relaxation during the acquisition of scans 001, 003 and 005 (the drop of the peak force was approximately 160 N, see Fig. 3). At the peak of the fourth loading cycle, the fast relaxation stage was followed by a more gradual decrease. During the acquisition of scan 007, the force decrease was approximately 50 N. Next, the normalized stroke was used as temporal basis. The results obtained with the two temporal interpolations are compared in the sequel. In both cases, only one DVC field was utilized as spatial mode, i.e., the displacement field of scan 007 (corresponding to the last loading cycle prior to specimen failure). This field was obtained by performing volumetric correlation between scans 0 (reference) and 007. It is important to emphasize that the P-DVC measurements were performed until specimen failure (i.e., *after* acquiring scan 007). The projections to be analyzed with P-DVC were selected so that the angle between two consecutive projections was equal to 5°. A total of 1,338 projections was analyzed (out of 17,442 radiographs acquired during the whole loading history), which led to 70 projections per turn (360° revolution). The chosen sampling was also governed by the computation time. In P-DVC procedures, the heaviest operations are the
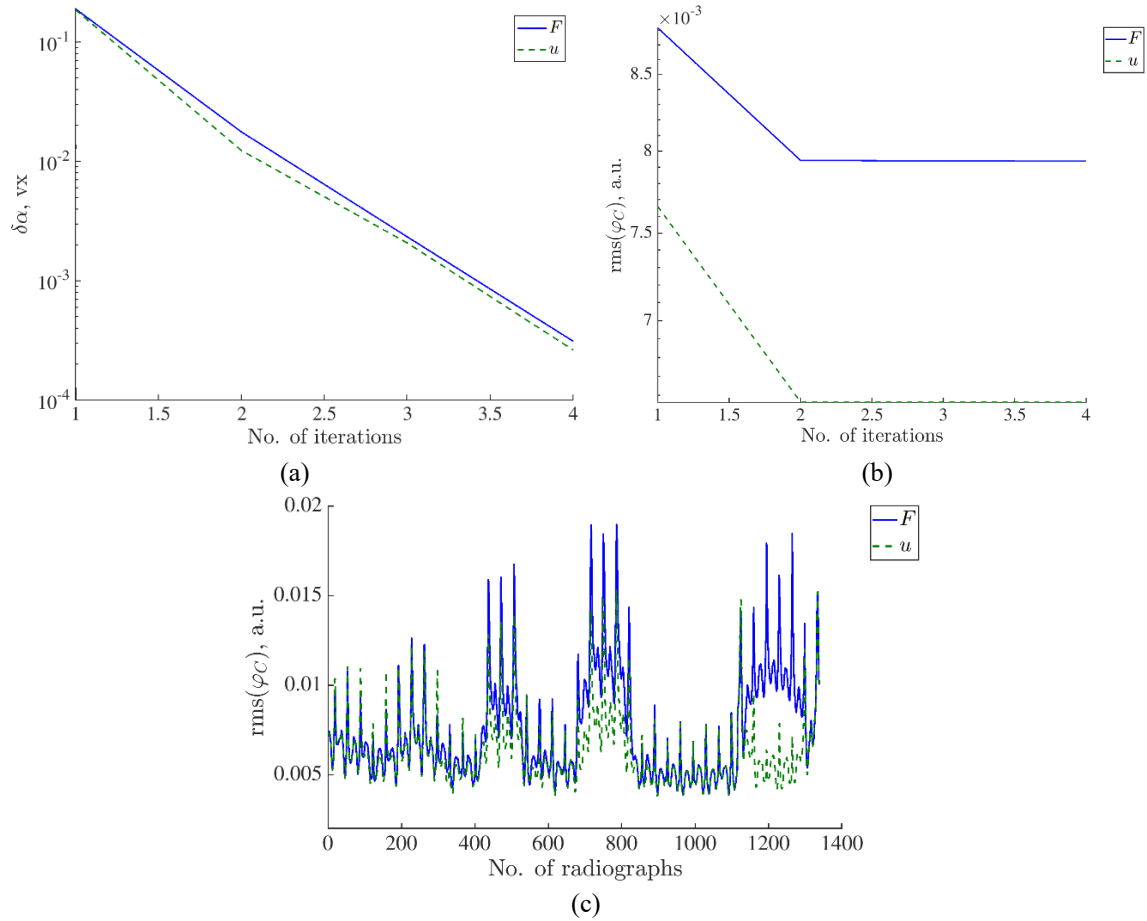
Fig. 6 (a) Change of displacement corrections $\delta\alpha$ during the iterative procedure. (b) Change of rms projection residuals over the entire Region of Interest during the iterative procedure. (c) Change of rms projection residuals at convergence for each analyzed radiograph over the entire loading history

computation of Hessian (i.e., sensitivity) matrices and the correction of the reference volume (Eqs. (11)-(12)). Thus, to perform measurements in reasonable time, a compromise had to be made between temporal resolution and computation time. Last, the initial value of α was set to 1 (Eq. (8)).

The convergence of the algorithm was first evaluated from the change of displacements corrections during the iterative procedure (Fig. 6(a)). Both analyses took 4 iterations to converge. The measured displacement fields yielded a global decrease of the residuals within the inspected ROI, as shown in Fig. 6(b). Using the stroke history resulted in a significantly lower global residual. The same conclusions are drawn when observing the rms residual for each analyzed angle/time-step (to be compared with the mean dynamic range of original radiographs (0.7. a.u.)) shown in Fig. 6(c). Their differences were especially pronounced in the unloaded stages of the conducted experiment (Fig. 3). The residuals obtained using the stroke history remained lower during the analyzed loading history, while those obtained using the measured force signal were higher in unloaded stages. In both analyzed cases, the peaks of the rms residuals were observed for

Table 2 Converged temporal amplitudes α obtained with the two temporal interpolations

Signal	F	U
Initial α	1	1
Converged α	1.206	1.197

Table 3 Comparison of rms differences in *z* direction between the 3D nodal displacements measured from the registration of two 3D images (with FE-DVC, see Fig. 3) and projection-based measurements. The comparison was performed for converged P-DVC displacement fields for the angles at the beginning of each constant stroke stage

		rms(U_z^{DVC}-$u_z^{\text{P-DVC}}$), vx	
Scan	Mechanical state	F	U
000	Unloaded	0.05	0.05
001	Loaded	0.81	0.05
002	Unloaded	0.35	0.06
003	Loaded	0.88	0.06
004	Unloaded	1.56	0.22
005	Loaded	0.73	0.08
006	Unloaded	2.77	0.30
007	Loaded	0.78	0.09
008	Unloaded	3.76	0.25

the radiographs acquired at 90º and 270º degrees with respect to the detector (as the thickness of the specimen with respect to the X-ray source was the highest).

The comparison of the two temporal interpolations was performed with the converged value of α (Eq. (10)). The amplitude α was very close in both cases (Table 2), and greater than 1, since the DVC displacement field of the last loading cycle prior to specimen failure was used as spatial mode (Fig. 3), while the 4D characterization was performed beyond this stage (i.e., up to the specimen failure). Thus, despite this *extrapolation*, the displacement fields for all analyzed radiographs converged and were consistent (Fig. 6). With the chosen temporal sampling, the kinematics was very well captured even though with the increase in load levels the displacement fields became more heterogeneous.

Furthermore, the rms differences between the 3D nodal displacements measured from the registration of two 3D images (with FE-based DVC) and projection-based measurements were calculated only for displacements in the *z* (i.e., loading) direction. The DVC displacement fields of the scans acquired during the prescribed loading history were obtained by performing volumetric correlations with scan 0 being the reference. It is important to highlight that large rigid body rotations (RBRs) in *x* and *y* directions were observed during the experiment. Thus, the rms differences were only computed for *z* direction displacements as the mechanical component was dominant in that direction. The rms differences were calculated between DVC displacement fields and converged P-DVC displacement fields for the time-steps corresponding to the beginning of each constant stroke stage (Table 3). As the series of projections acquired at the maximum load levels were affected by time-dependent motions (i.e., stress-relaxation phenomena), which influenced the reconstruction of the full volume, differences were expected. From the values
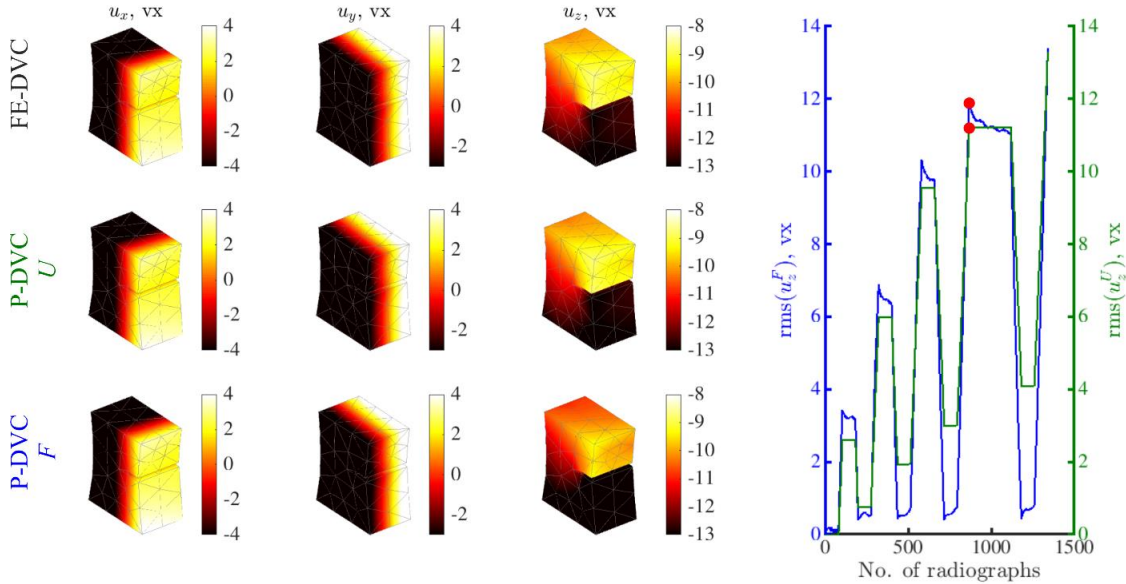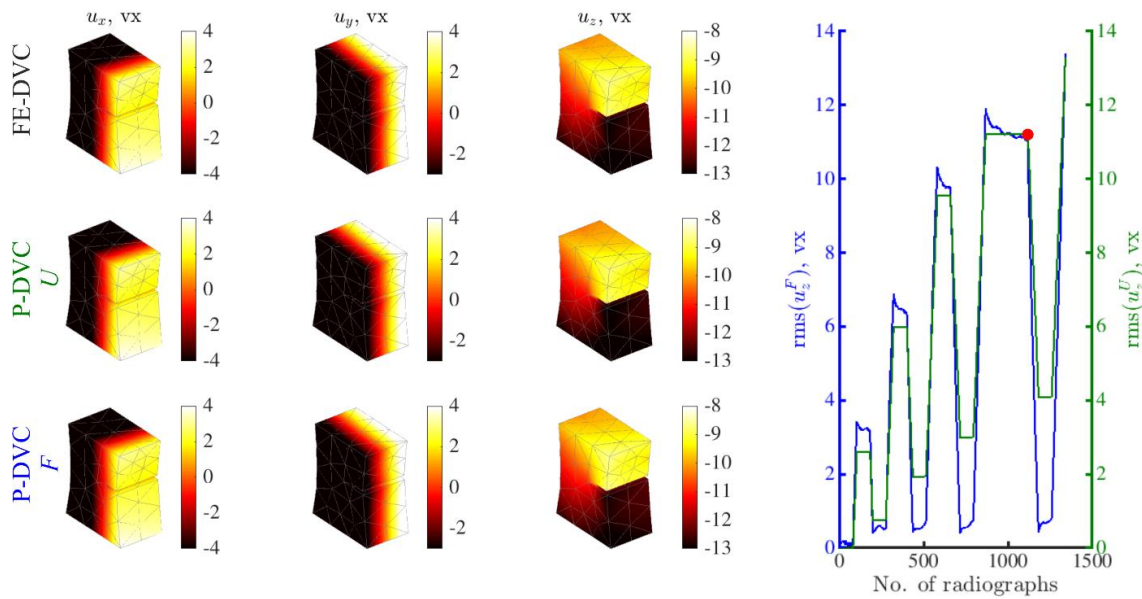
Fig. 7 Comparison of displacement fields at the beginning of the last loading cycle (projection 865) prior to specimen failure obtained with DVC (top) and P-DVC using the stroke history (middle) or measured uniaxial force (bottom) as temporal basis. The red dots on rms ($u_z^{P,DVC}$) using the measured uniaxial force (blue) and prescribed stroke history (green) marks the time-step at which the results were compared

reported in Table 3, it is concluded that for both temporal regularization procedures the rms differences were higher for the unloaded stages of the conducted experiment (which was especially pronounced when using the measured uniaxial force as the temporal interpolation basis). This was due to the fact that part of the deformation mechanisms was deactivated (Vrgoč *et al.* 2023). For the loaded stages, the differences were very small. This observation confirms that, despite using only one spatial mode (i.e., the displacement field of scan 007) when performing 4D measurements, the kinematics was very well captured. In addition, employing the stroke history as the temporal interpolation better captured the temporal fluctuations (as the rms differences were smaller compared to those obtained when using the measured uniaxial force).

The displacement fields at the beginning of the last loading cycle obtained with P-DVC employing both temporal interpolations are shown in Fig. 7. They correspond to time-step 865 and are compared to the FE-DVC field of scan 007. From the presented displacement fields, it is seen that RBRs occurred during the conducted cyclic tensile test. The comparison of displacement fields further confirmed that the kinematics was properly captured at this stage with the P-DVC framework employed herein. However, higher differences in the *z* direction displacement fields were observed when performing P-DVC employing the measured force as temporal basis (Table 3).

To further analyze the latter statement, Table 4. reports the rms differences in *z* direction between the projection-based measurements at the beginning (time-step 865) and the end (time-step 1115) of the last loading cycle prior to specimen failure and displacement field of scan 007 obtained with DVC. At the beginning of the last loading cycle prior to specimen failure, using the measured uniaxial force as the temporal basis resulted in higher rms displacement difference. At the end of the loading cycle, this rms difference significantly decreased and reached the level obtained by using the stroke history as temporal basis (which was constant through the loading

Table 4 Comparison of rms differences *in* z direction between the nodal displacements measured from the registration of two 3D images (with FE-DVC, see Fig. 3) and projection-based measurements for the beginning (time-step 865) and the end (time-step 1115) of the last loading cycle prior to specimen failure

	Time-step 865		Time-step 1115	
	rms (U_z^{DVC}-$u_z^{\text{P-DVC}}$), vx		rms (U_z^{DVC}-$u_z^{\text{P-DVC}}$), vx	
Scan	F	U	F	U
007	0.78	0.09	0.09	0.09

Fig. 8 Comparison of displacement fields at the end of the last loading cycle (time-step 1115) prior to specimen failure obtained with DVC (top) and P-DVC using the stroke history (middle) and measured uniaxial force (bottom) as temporal basis. The red dots on the rms ($u_z^{\text{P.DVC}}$) using the measured uniaxial force (blue) and prescribed stroke history (green) marks the time-step at which the results were compared

plateau). This effect stems from the fact that the measured uniaxial force revealed relaxation phenomena, and thus, the projection-based measured displacements differed. Conversely, the stroke history was constant (Fig. 3) and thus the projection-based displacements were constant during the analyzed loading.

Fig. 8 shows the displacement fields at the end of the last loading cycle obtained with P-DVC employing both temporal interpolations. These fields correspond to time-step 1115 and are compared to FE-DVC fields of scan 007. At the end of the loading cycle the differences between the projection-based and DVC fields of scan 007 are negligible (which is further confirmed by the values reported in Table 4).

Fig. 9 displays the projection residual map and major eigen strain field when θ=105° captured at very end of the analyzed loading history, i.e., just before specimen failure. This map was obtained via P-DVC employing the stroke history as temporal basis. The measured displacement field correctly reduced the residual and thus was deemed trustworthy. Some residuals are still visible within the inspected ROI. The elevated residuals in the notched region were expected to
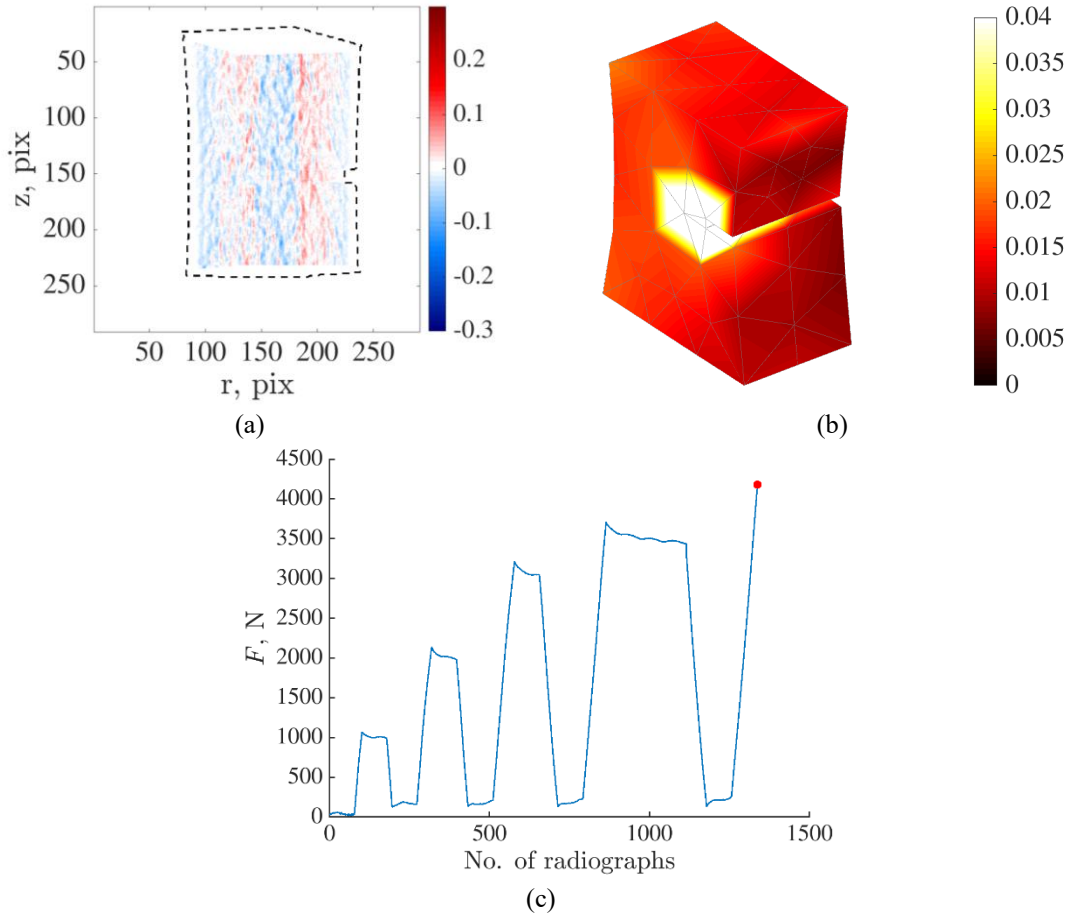
Fig. 9 (a) Projection residual map and (b) major eigen strain field obtained with P-DVC employing the stroke history as temporal basis calculated at the end of the analyzed loading history (time-step 1338), i.e., just before specimen failure. (c) Measured uniaxial force history. The red dot denotes the time step 1338 at which the residual map and major eigen strain field are shown

occur as high strain gradients appeared in this region (Fig. 9(b)). In a previous work (Vrgoč *et al.* 2023), when only DVC measurements were used, it was shown that multiple cracks initiated and propagated within the notched region.

5. Conclusions

In the present work, 4D mechanical characterization of a glass fiber mat reinforced polyester resin was performed by employing P-DVC enhanced DVC that relied on space-time discretization of measured displacement fields. An alternative route in which spatial modes are constructed with DVC, and only temporal modes were sought via P-DVC was exploited. The main conclusions are as follows:

    • By continuously acquiring the radiographs over the entire loading history and using only one

radiograph per loading step, it was possible to enrich the temporal sampling compared to scan-wise DVC. Within such a framework, it may be possible to capture time-dependent phenomena such as e.g., stress-relaxation and crack propagation.

• The 4D kinematics was measured using two different temporal bases (i.e., the normalized stroke history or normalized measured uniaxial force). In both cases, only one spatial mode was used, namely, the displacement field of scan 007 (corresponding to the peak of the last loading cycle prior to specimen failure) measured via FE-DVC. It is important to note that 4D displacement fields were measured beyond the last loading cycle (up to specimen failure). Despite this extrapolation, the kinematics was very well captured (even though with the increase in load levels the displacement fields became more heterogeneous). These results prove that using only one spatial mode was sufficient to measure the entire 4D kinematics.

• Both temporal interpolations led to a global decrease of the residuals over the entire ROI. Thus, the measured displacement fields correctly reduced the residual and were deemed trustworthy. However, using the stroke history resulted in a significantly lower global residual.

One of the principal aspects of future investigations will be the enrichment of the temporal basis and thus the spatial modes to further probe the solution faithfulness. The presented results were obtained using coarse grained images (i.e., the resulting definition was down-sampled over a 4×4 regular square grid). This may lead to a loss of information beneficial for mechanical characterization. Another aspect will thus be to perform 4D measurements at the original scale. In addition, the measurements may be improved by further adjusting the geometrical parameters of the tomography setup, as well as performing beam hardening corrections (which was not carried out in the current work). The final objective will be to characterize time-dependent phenomena, especially the inception and propagation of damage as a previous work (Vrgoč *et al.* 2023) revealed damaged zones within the investigated specimen via DVC residual fields.

Acknowledgments

References

Bartulović, A., Tomičević, Z., Bubalo, A. and Hild, F. (2022), "Assessment of DVC measurement uncertainty on GFRPs with various fiber architectures", *Couple. Syst. Mech.*, **11**(1), 15-32. https://doi.org/10.12989/csm.2022.11.1.015.

Brunner, A. (2018), "Identification of damage mechanisms in fiber-reinforced polymer-matrix composites with acoustic emission and the challenge of assessing structural integrity and service-life", *Constr. Build. Mater.*, **173**, 629-637. https://doi.org/10.1016/j.conbuildmat.2018.04.084.

Buljac, A., Jailin, C., Mendoza, A., Neggers, J., Taillandier-Thomas, T., Bouterf, A., ... & Roux, S. (2018),

"Digital volume correlation: Review of progress and challenges", *Exp. Mech.*, **58**, 661-708. https://doi.org/10.1007/s11340-018-0390-7.

Buljac, A., Navas, V.M.T., Shakoor, M., Bouterf, A., Neggers, J., Bernacki, M., ... & Hild, F. (2018), "On the calibration of elastoplastic parameters at the microscale via x-ray microtomography and digital volume correlation for the simulation of ductile damage", *Eur. J. Mech. A-Solid.*, **72**, 287-297. https://doi.org/10.1016/j.euromechsol.2018.04.010.

Jailin, C., Buljac, A., Bouterf, A., Hild, F. and Roux, S. (2018), "Fast four-dimensional tensile test monitored via X-ray computed tomography: Single projection-based Digital Volume Correlation dedicated to slender samples", *J. Strain Anal.*, **53**(7), 473-484. https://doi.org/10.1177/0309324718797765.

Jailin, C., Buljac, A., Bouterf, A., Poncelet, M., Hild, F. and Roux, S. (2018), "Self-calibration for lab-μct using space-time regularized projection-based DVC and model reduction", *Meas. Sci. Technol.*, **29**, 024003. https://doi.org/10.1088/1361-6501/aa9818.

Leclerc, H., Neggers, J., Mathieu, F., Hild, F. and Roux, S. (2015), Correli 3.0, Agence pour la Protection des Programmes, Paris, France, IDDN.FR.001.520008.000.S.P.2015.000.31500.

Maurer, J., Jerabek. M., Salaberger, D., Thor, M., Kastner, J. and Major, Z. (2022), "Stress relaxation behaviour of glass fibre reinforced thermoplastic composites and its application to the design of interrupted in situ tensile tests for investigations by X-ray computed tomography", *Polym. Test.*, **109**, 107551. https://doi.org/10.1016/j.polymertesting.2022.107551.

Prashanth, S., Km, S. and Nithin, K. (2017), "Fiber reinforced composites-A review", *J. Mater. Sci. Eng.*, **6**, 1-6. https://doi.org/10.4172/2169-0022.1000341.

Tomičević, Z., Bouterf, A, Surma, R. and Hild, F. (2019), "Damage observation in glass fiber reinforced composites", *Mater. Today: Proc.*, **12**(2), 185-191. https://doi.org/10.1016/j.matpr.2019.03.093.

van Aarle, W., Palenstijn, W.J., De Beenhouwer, J., Altantzis, T., Bals, S., Batenburg, K.J. and Sijbers, J. (2015), "The ASTRA Toolbox: A platform for advanced algorithm development in electron tomography", *Ultramicroscopy*, **157**, 35-47. https://doi.org/10.1016/j.ultramic.2015.05.002.

Vrgoč, A., Tomičević, Z., Smaniotto, B. and Hild, F. (2021), "Damage characterization in fiber reinforced polymer via Digital Volume Correlation", *Couple. Syst. Mech.*, **10**(6), 545-560. https://doi.org/10.12989/csm.2021.10.6.545.

Vrgoč, A., Tomičević, Z., Smaniotto, B. and Hild, F. (2023), "Characterization of glass fiber reinforced polymer via Digital Volume Correlation: Investigation of notch sensitivity", *Mech. Mater.*, **177**, 104552. https://doi.org/10.1016/j.mechmat.2022.104552.